www.ietdl.org

Published in IET Microwaves, Antennas & Propagation
Received on 9th February 2010
Revised on 23rd May 2011
doi: 10.1049/iet-map.2010.0050

ISSN 1751-8725

Design and optimisation of a novel dual-band circularly polarised microstrip antenna

Md. Gaffar M.A. Zaman S.M. Choudhury Md.A. Matin

Department of Electrical and Electronic Engineering, Bangladesh University of Engineering and Technology, Dhaka, Bangladesh
E-mail: gaffareeebuet@gmail.com

Abstract: A novel dual-band circularly polarised patch feed antenna is presented. It is theoretically analysed and simulated. It is optimised with a genetic algorithm (GA) which is capable of producing an antenna design that has a low voltage standing wave ratio (VSWR), low cross-polarisation and large bandwidths but small dimensions. A hybrid finite-element method/method of moment model was used to simulate the proposed antenna in which 1.54% axial ratio bandwidth was obtained. Both the effectiveness of the optimisation methodology and the proposed antenna configuration have been scrutinised by simulation and theoretical analysis.

1 Introduction

Since truncated microstrip antennas are small, light weight, low cost and can easily produce circular polarisation (CP), they have found widespread application in satellite and wireless mobile communication systems [1, 2]. Several circularly polarised microstrip antennas have been investigated over the past two decades [2, 3]. A number of different structures have been proposed [4] to improve the performance of circularly polarised antennas (diagonal-fed nearly square, corner-truncated square and diagonal-slot square [5]). They exhibit a low axial ratio (AR, defined as the ratio of the major to minor axes of a polarisation ellipse) bandwidth and have stringent manufacturing tolerances. To improve the AR, impedance and power bandwidth [6] and also to reduce size and create multi-band performance, many methods have been proposed by researchers. Some of these methods include stacked structure [7], closely spaced parasitic patches [8], lossy dielectric material [9], shorting pins [10], slotted patches of different shape [11], photonic band gap structure [12], dielectric superstrate, single-layer [13] and multilayer [14] synthetic substrate etc. In 1997, Wong *et al.* presented an experimental study of a novel circularly polarised slotted square microstrip antenna with a dimension: 30 mm × 30 mm, a resonant frequency of orthogonal modes at 1849 MHz and an AR bandwidth of 24 MHz (1.3%) [15] which was larger than conventional ones [4]:

1. Huang *et al.* [16] presented a similar antenna in 1998. However that antenna had a high permittivity ($\varepsilon_r = 79$) ceramic superstrate. The dimension of that antenna was 26.2 mm × 26.2 mm which is 30% smaller than conventional design [4]. The antenna had a resonant frequency of 2697 MHz with AR bandwidth of 1.4%. A combined type of CP antenna was presented in [17]. It has dimension of 28 mm × 28 mm, and resonant frequency 1970 MHz, better AR bandwidth and 36% size reduction than [4].

In this paper, a novel dual-band circularly polarised unequal T-slotted microstrip antenna with dimension 25 mm × 25 mm is presented for dual-band operation [18, 19]. It has resonant frequencies at 2069.2 and 2210.3 MHz, both with a VSWR of 2, an impedance bandwidth of 45 MHz (2.2%) and an AR bandwidth of 32 MHz (1.54%). The dimensions are 42% smaller than the structure in [4]. In this study, a hybrid finite-element method/method of moment (FEM/MoM) technique is applied to analyse the proposed CP microstrip antenna. Section 2 briefly describes the hybrid FEM/MoM approach, how the antenna is modelled, and how the scattering parameters are calculated. Section 3 presents the genetic algorithm (GA) which is used for increasing input gain at nearly degenerate resonance frequencies and lowering the cross-polarisation. Section 4 summarises several application criteria, limitations and outlines directions for future research on this antenna structure.

2 Method of analysis and simulation

A microstip antenna consists of a radiating patch (lossy metal), metal ground and a substrate between them. To excite the patch metal, a probe-feed coaxial cable is used. An incident wave ($\boldsymbol{E}^{\text{inc}}, \boldsymbol{H}^{\text{inc}}$) or an impressed current source $\boldsymbol{J}^{\text{int}}$ impinges from the coaxial cable to the patch. The field equations are modelled by using FEM to solve the weak form of the vector wave equation as follows [20]

$$\int_V \left[\left(\frac{\nabla \times \boldsymbol{E}(\boldsymbol{r})}{\mathrm{j}w\mu_0\mu_{\bar{r}}} \cdot (\nabla \times \boldsymbol{f}(\boldsymbol{r})) \right) + \mathrm{j}w\varepsilon_0\varepsilon_r \boldsymbol{E}(\boldsymbol{r}) \cdot \boldsymbol{f}(\boldsymbol{r}) \right] \mathrm{d}V = \int_S (\hat{n} \times \boldsymbol{H}(\boldsymbol{r})) \cdot \boldsymbol{f}(\boldsymbol{r})\, \mathrm{d}S - \int_V \boldsymbol{J}^{\text{int}}(\boldsymbol{r}) \cdot \boldsymbol{f}(\boldsymbol{r})\, \mathrm{d}V \quad (1)$$

where S is the surface enclosing volume V and $\boldsymbol{f}(\boldsymbol{r})$ is the testing function. The electric field can be approximated by

using the tetrahedral element $\boldsymbol{w}(\boldsymbol{r})$

$$\boldsymbol{E}(\boldsymbol{r}) \simeq \sum_{k=1}^{M} (\boldsymbol{E}_i)_k \boldsymbol{w}_k(\boldsymbol{r}) + \sum_{n=1}^{N} (\boldsymbol{E}_s)_n \boldsymbol{w}_n(\boldsymbol{r})$$

where $\boldsymbol{E}_i$ and $\boldsymbol{E}_s$ are sets of unknowns for the electric field within the volume V and on the surface S. M and N are the number basis functions within the volume and on the surface. The tangential magnetic field can be expanded using a basis function

$$\hat{n} \times \boldsymbol{H}(\boldsymbol{r}) \simeq \sum_{n=1}^{N} (\boldsymbol{J}_s)_n \boldsymbol{f}_n(\boldsymbol{r})$$

where J_s is a set of unknowns for the equivalent electric current on the surface S. A Galerkin method can be used to discretise (1) as follows [20]

$$\begin{bmatrix} \boldsymbol{G}_{ii} & \boldsymbol{G}_{is} \\ \boldsymbol{G}_{si} & \boldsymbol{G}_{ss} \end{bmatrix} \begin{bmatrix} \boldsymbol{E}_i \\ \boldsymbol{E}_s \end{bmatrix} = \begin{bmatrix} 0 & 0 \\ 0 & \boldsymbol{H}_{ss} \end{bmatrix} \begin{bmatrix} 0 \\ \boldsymbol{J}_s \end{bmatrix} + \begin{bmatrix} g_i \\ g_s \end{bmatrix}$$

where $\boldsymbol{G}_{ii}$, $\boldsymbol{G}_{is}$, $\boldsymbol{G}_{si}$, $\boldsymbol{G}_{ss}$ and $\boldsymbol{H}_{ss}$ are unknown coefficient matrices and g_i and g_s are source terms.

The exterior electric field can be represented via an electric field integral equation (EFIE) [21–22]

$$\frac{\boldsymbol{E}(\boldsymbol{r})}{2} = \boldsymbol{E}^{\text{inc}}(\boldsymbol{r}) + \int_S \begin{bmatrix} -\boldsymbol{M}(\boldsymbol{r}') \times \nabla' G_0(\boldsymbol{r}, \boldsymbol{r}') \\ + j\dfrac{\eta_0}{k_0} \nabla' \cdot \boldsymbol{J}(\boldsymbol{r}') \nabla' G_0(\boldsymbol{r}, \boldsymbol{r}') \end{bmatrix} \mathrm{d}S'$$

where $\boldsymbol{J}(\boldsymbol{r})$ and $\boldsymbol{M}(\boldsymbol{r})$ in the above equation are the equivalent surface electric and magnetic currents which can be approximated as follows

$$\boldsymbol{J}(\boldsymbol{r}) = \hat{n} \times \boldsymbol{H}(\boldsymbol{r}) \simeq \sum_{n=1}^{N} (\boldsymbol{J}_s)_n f_n(\boldsymbol{r})$$

$$\boldsymbol{M}(\boldsymbol{r}) = \boldsymbol{E}(\boldsymbol{r}) \times \hat{n} \simeq \sum_{n=1}^{N} (\boldsymbol{E}_s)_n f_n(\boldsymbol{r})$$

After discretising the EFIE, the MoM matrix equation is in the following form

$$[\boldsymbol{C}][\boldsymbol{J}_s] = [\boldsymbol{D}][\boldsymbol{E}_s] - [\boldsymbol{F}^i]$$

where $[\boldsymbol{C}]$ and $[\boldsymbol{D}]$ are the coefficient matrices, and $[\boldsymbol{F}^i]$ is the excitation term. The FEM and MoM equations are coupled by enforcing the continuity of the tangential fields on the boundary, such as for the PEC boundary condition $\hat{n} \times \boldsymbol{E} = 0$ must be enforced.

The probe model represents the feed as a current filament along the centre conductor of the coaxial cable. An impressed current source along the z-axis can be expressed as

$$\boldsymbol{J}^{\text{int}} = I_1 \delta(x - x_{\text{f}}) \delta(y - y_{\text{f}}) \hat{Z}$$

where $(x_{\text{f}}, y_{\text{f}})$ represents feed point (6 mm, 0), $\boldsymbol{I}_1$ denotes the electric current magnitude and $\delta(x)$ is the Dirac delta function.

The FEM/MoM method can be used to analyse the scattering parameters (S-parameters) of a two-port electromagnetic system. The characteristic impedances of Ports 1 and 2 are Z_{c1} and Z_{c2}, respectively. In this study, both Ports 1 and 2 are matched at the resonant frequency and set to 50 Ω. Port 1 is driven by a current source I_s with source impedance Z_s and terminated at Port 2 by a load Z_2. Thus, we can calculate the S_{11} value as follows

$$S_{11} = \frac{(Z_s + Z_{c1})V_1 - Z_{c1}Z_s I_s}{Z_{c1}Z_s I_s + (Z_s - Z_{c1})V_1}$$

where V_1 is the port voltage.

Fig. 1 shows the proposed single-feed square microstrip antenna for compact CP operation. The square microstrip patch has a side length L (25 mm) and is printed on a substrate FR4 ($\varepsilon_r = 4.4$) of thickness t (1.6 mm). The T-slots are of unequal lengths a (5.5 mm) and b (6.5 mm) with $M = N = 8\sqrt{2}$ mm but have equal widths w (1 mm) and are inserted at the four patch corners, with an angle $\phi = \pm 45^\circ$ with respect to base. The truncated corners are of equal side length S (5 mm). The single probe feed is placed at point x (6 mm) on the X-axis for RHCP operation.

To achieve reduced-size and dual-band CP operation [18], slits and truncated corners are used. Owing to the slits, the equivalent excited patch surface current path is lengthened. Thus, it reduces the resonant frequency of the patch. From Fig. 2, the impedance bandwidth is 32 MHz at 2069.2 MHz and 45 MHz at 2210.3 MHz [measured at below 10 dB return loss (RL)]. A reasonable meshing and iteration have been carried out to find out the approximate resonant frequency. RHCP operation can be seen in Fig. 3 which is also normalised with the maximum gain value and Figs. 4 and 5 show an AR bandwidth of 33.5 MHz at 2069 MHz and 32 MHz at 2233 MHz. Although the axial ratio bandwidth of a CP antenna should stay within the boundary of impedance bandwidth but in this paper, AR bandwidth of our proposed CP antenna approximates the real one [18]. Here, hybrid FEM/MoM uses adaptive meshes to improve the simulation design.

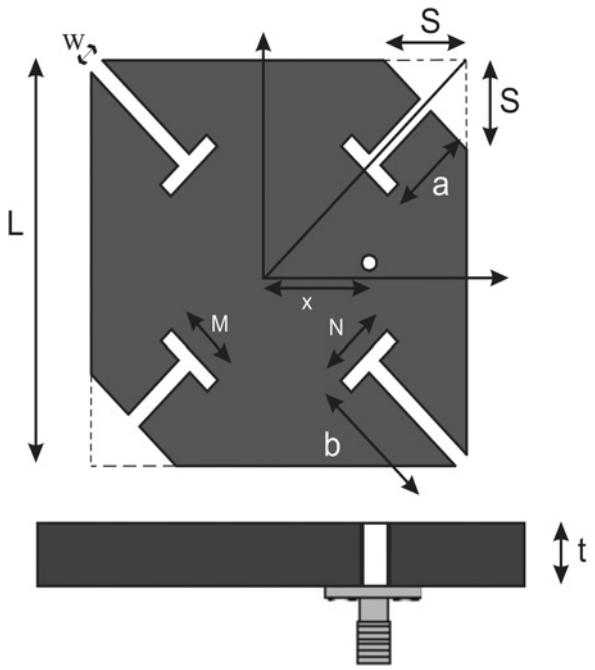

Fig. 1 *Proposed microstrip antenna where $x = 6$ mm, $L = 25$ mm, $t = 1.6$ mm, $a = 5.5$ mm, $b = 6.5$ mm, $M = N = 8\sqrt{2}$ mm, $w = 1$ mm and $S = 5$ mm*

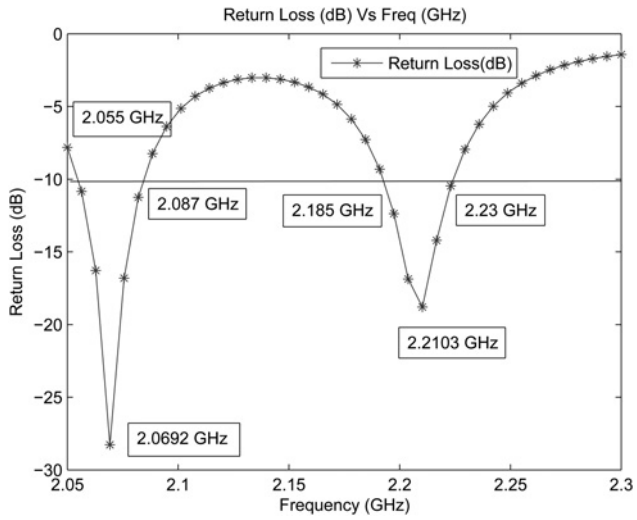

Fig. 2 *RL (dB) against frequency*

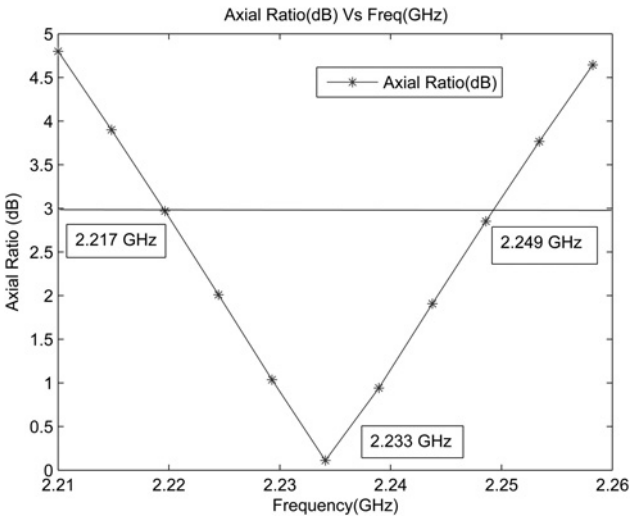

Fig. 5 *AR (dB) against frequency*

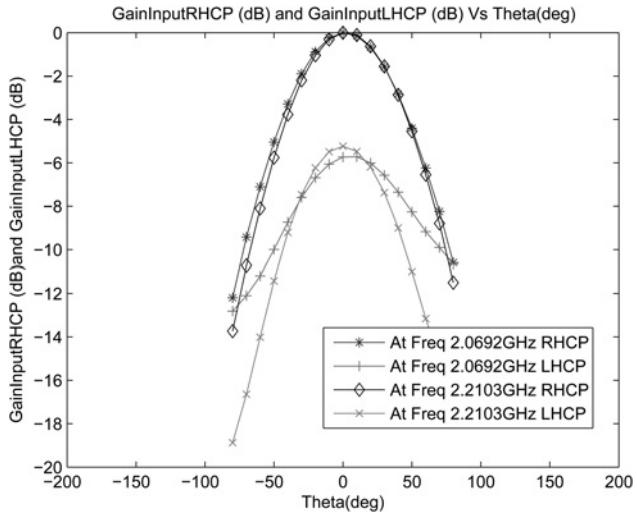

Fig. 3 *Gain input RHCP (dB) and gain input LHCP (dB) against theta where computed patterns are normalised at $\phi = 0$ plane*

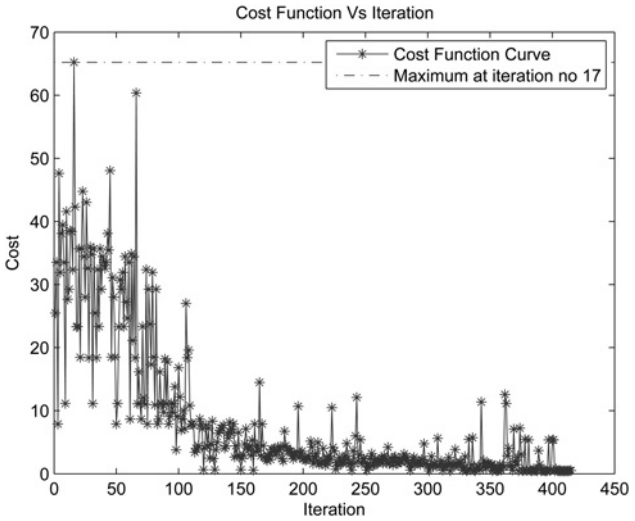

Fig. 6 *Cost against iteration in GA*

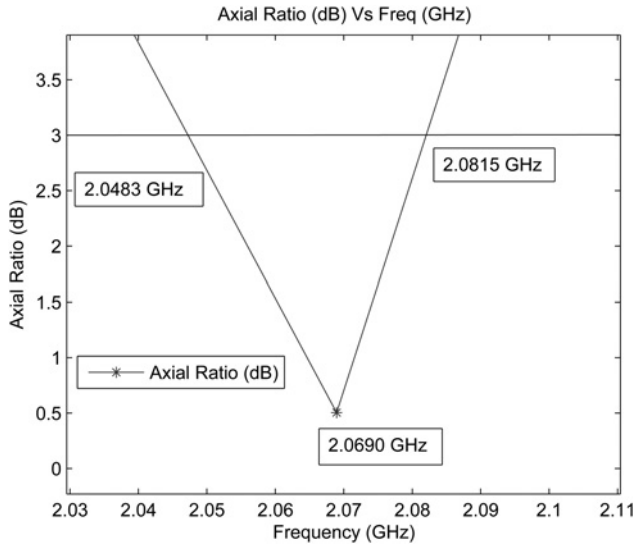

Fig. 4 *AR (dB) against frequency*

Owing to slit loading, a new excited mode denoted as $TM_{\delta 0}$ ($1 < \delta \leq 2$) can be excited near the fundamental mode of TM_{10}. These two modes, $TM_{\delta 0}$ and TM_{10}, are of the same polarisation plane and similar radiation characteristics and can be excited with an impedance-matched single feed. Since an unequal T-slot is embedded at the corners, its output gain differs at the two resonant frequencies. Using a single probe-feed at the x-axis or y-axis of the antenna, both perturbed TM_{10} and $TM_{\delta 0}$ modes can be split into two near-degenerate modes for dual-band CP operation [23]. To improve our initial design, 'a genetic algorithm' optimisation method has been implemented. In the next section, this optimisation method is described.

3 Optimisation

GAs are on the rise in electromagnetics as design tools and problem solvers because of their versatility and ability to optimise in complex multivariate searches [24–27].

By definition, genetic algorithms are methods for seeking extrema of a given objective function or cost function $f(s)$ where $s = \{s_l |\ l = 1, 2, 3, \ldots, N_x\}$. In design problems, the cost function describes the important features that measures

doi: 10.1049/iet-map.2010.0050

the system performance to be either maximised or minimised. For the advantage of simultaneous optimisation, antenna parameters which are inter-related each other can be optimised efficiently. In general, a GA does not operate directly on the parameter vector s but on a symbolic representation p of s, known as a chromosome. A chromosome is a collection of genes which decode to s_l, and is symbolically denoted as

$$\boldsymbol{p} = \{g_i | i = 1, 2, 3, \ldots, N_{g1}\}$$

where N_{g_l} is the genetic length and there is a corresponding relationship between the s_l and g_l given by

$$p \leftrightarrow \overbrace{g_1\, g_2\, g_3 \cdots g_{N_1}}\, \overbrace{g_{N_1+1} g_{N_1+2} g_{N_1+3} g_{N_1+3} \cdots g_{N_2}}$$

Genetic algorithms do not work on a single chromosome at a time, but on a whole population of N_{pop} chromosome for improving objective function values

$$\boldsymbol{P} = \{p_k | k = 1, 2, 3, \ldots, N_{\text{pop}}\}$$

where genes relate to the variables that are given in a information table. For each gene, 7 bits are required to encode the GA variables. A random selection of different behaviour is taken as samples. As the position of the feed shifts to a higher position along the x-axis, it comes near the edge of the T-slot. It causes more cross polarisation which decreases the cost function. The same occurs when the truncated portion or length of T-slot is large enough to come near to the edge of the feed position. For this reason, at higher iteration numbers the cost function decreases from a higher value to a lower value as shown in Fig. 5. For a given population $P^k = \{p_i^k, i = 1, 2, 3, \ldots, N_{\text{pop}}\}$, a single GA iteration starts by evaluating the vector $F^k = \{f_i^k : i = 1, 2, 3, \ldots, N_{\text{pop}}\}$ of cost function values f_i^k associated with chromosomes p_i^k. The cost function is as follows for low cross-polarisation

$$F = \text{minimisation of} \left\{ W_1 \times \left(\frac{1}{\text{VSWR}} \right) + \sum_{i=2}^{n} W_i \times \text{AR}_i \right\}$$

where $\text{VSWR} = (1 + |\Gamma|)/(1 - |\Gamma|)$, AR_i is the ith axial value at elevation angle θ_i (at $\phi = 0$ plane), and n is the number of elevation angles required. W_1 and W_i are the weight coefficients for the cost function that were optimised according to the target objectives set by the design. W_i are the primary values that were considered to have a rescannable wide elevation variation AR.

The GA then applies the genetic operators of selection, crossover and mutation to P^k to produce P^{k+1}. With the creation of P^0, the population enters the main GA loop which is iterated on each successive population P^k. Generic manipulation of P^k begins with the selection of best chromosomes on the basis of cost function values F^k. Selection processes include roulette-wheel selection, ranking selection, stochastic binary tournament selection. For our design we used stochastic binary tournament selection because binary tournament selection generally works faster than roulette-wheel selection, and it avoids convergence problems [28]. It chooses pairs of chromosomes from P^k and places the better ones in P^k_{selected} until it is replete.

Selection is followed by crossover, which serves to hybridise design traits by creating a new population $P_c^k = C(P^k_{\text{selected}})$, where $C()$ denotes as a crossover function. Thus, it can be stated as below

$$C(P^k_{\text{selected}}) = \bigcap_{i=1}^{N_{\text{pop}}/2} C[\text{ch}(p^k_{\text{selected}}), \text{ch}(p^k_{\text{selected}})]$$

where the operator 'ch(p)' chooses a random chromosome from P and the operator 'C' maps a pair of chromosomes, crossover is the main search tool of the GA since it combines chromosomes which contain genetic information which is known to be useful

$$p_1 = \{g_{1_j}, j = 1, 2, 3, \ldots, N_{g_l}\}$$

$$p_2 = \{g_{2_j}, j = 1, 2, 3, \ldots, N_{g_l}\}$$

According to the rule

$$C(p1, p2) = \begin{cases} \hat{p}_1, \hat{p}_2 & \text{with probability } P_{\text{cross}} \\ p_1, p_2 & \text{with probability } 1 - P_{\text{cross}} \end{cases}$$

where the hybrids $\hat{p}_1$ and $\hat{p}_2$ are given by

$$\hat{p}_1 = g_{11}, g_{12}, g_{13}, \ldots, g_{1k}, g_{2(k+1)}, \ldots, g_{2N_{gl}}$$

$$\hat{p}_2 = g_{21}, g_{22}, g_{23}, \ldots, g_{2k}, g_{1(k+1)}, \ldots, g_{1N_{gl}}$$

The initial set-up is the most important part of GA. To minimise the shift of resonant frequencies from 2063.2 and 2210.3 MHz, we have selected the optimisation range with some conditions such as AR and impedance bandwidth restrictions, and maximum shift of resonant frequency shift about 200 MHz [28–33]. Crossover probability was taken as high (65%) as possible for high comparison and the mutation probability (0.8%) was taken as low as possible for higher accuracy. Resonant frequencies shift towards the lower-frequency region (shown in Fig. 7) and the normalised input gain (dB) is shown in Fig, 8. Both impedance and AR bandwidth become the same as before because of small changes in the structure and conditions applied. At iteration 17 shown in Fig. 6, the cost function maximises, that is, it optimises the proposed antenna with minimum cross polarisation. Owing to increasing slot areas

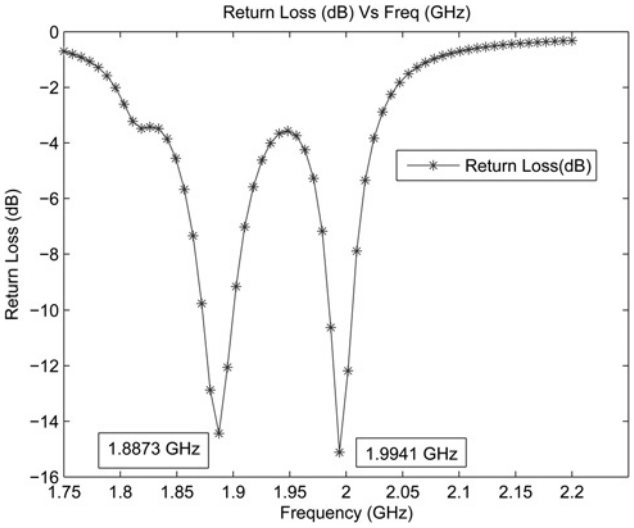

Fig. 7 *RL (dB) against frequency (GHz) after optimisation*

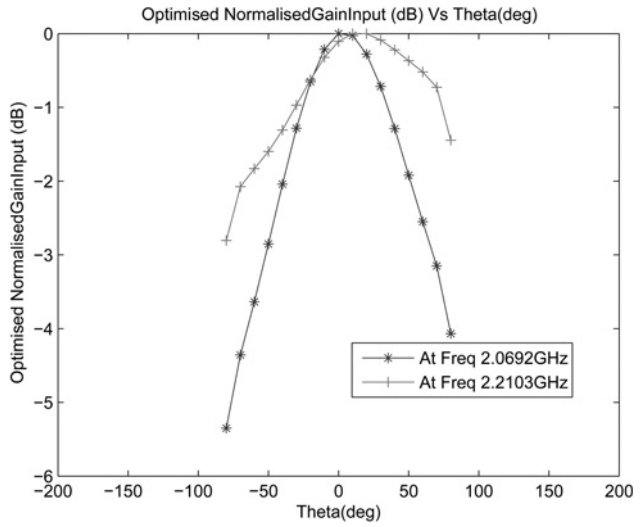

Fig. 8 *Normalised input gain (dB) against theta where computed patterns are normalised at $\phi = 0$ plane*

on the patch, the cost function becomes worse in the later iterations.

4 Conclusion

An approach to model a CP microstip antenna using a hybrid FEM/MoM method along with an evolutionary optimisation scheme GA has been presented. FEM is used to model the details of the structure and feed. MoM is used to provide a radiation boundary condition to terminate the FEM mesh. The excitation of a pair of two near-degenerate resonant modes for dual-band CP operation is achieved by inserting a T-slot and corner-truncated portion. Compared with the conventional corner-truncated antenna square microstrip antenna [4], the proposed compact dual-band CP design results in a large antenna dimension reduction (about 42%), better impendence and AR bandwidth (1.54%) and a relaxed manufacturing tolerance owing to the increase of required perturbation area. Therefore the proposed antenna is essentially attractive for wireless applications in a multipath environment. It is also well suited to compact and low-cost active circuit applications at microwave frequencies and RF front-end antenna integration.

5 Acknowledgment

This work was supported by Bangladesh University of Engineering and Technology (BUET).

6 References

1 Lee, K.F., Chen, W.: 'Advances in microstrip and printed antennas' (John Wiley Sons, USA, Canada, 1997)
2 James, J.R., Hall, P.S., Wood, C.: 'Microstrip antenna theory and design' (Peter Peregrinus, London, UK, 1981)
3 Garg, R., Bhartia, P., Bhal, I., Ittipiboon, A.: 'Microstrip antenna design handbook' (Artech house, Norwood, MA, 1995)
4 Sharma, P.C., Gupta, K.C.: 'Analysis and optimized design of single feed circularly polarized microstrip antenna', *IEEE Trans. Antennas Propag.*, 1983, **29**, pp. 945–955
5 Aksun, M.I., Shuang, S.L., Lo, Y.T.: 'On slot-coupled microstrip antennas and their applications to cp operation theory and experiment', *IEEE Trans. Antennas Propag.*, 1990, **38**, pp. 1224–1230
6 Langston, W.L., Jacson, D.R.: 'Impedance, axial ratio and receive-power bandwidths of microstrip antennas', *IEEE Trans. Antennas Propag.*, 2004, **52**, pp. 2769–2774
7 Lee, R.Q., Lee, K.F., Bobinchak, J.: 'Characteristics of two layer electromagnetically coupled rectangular patch antenna', *Electron. Lett.*, 1987, **23**, pp. 1070–1072
8 Chen, W., Lee, K.F., Lee, R.Q.: 'Spectral domain moment method analysis of co-planner micrsostrip parasitic subarrays', *Microw. Opt. Technol. Lett.*, 1993, **6**, pp. 157–163
9 Pan, K.H., Berhard, J.T., Moore, T.: 'Effects of lossy dielectric materials on microstrip antennas'. Proc. IEEE AP-S Conf. Antennas and Propagations In Wireless Communications, November 2000, pp. 39–42
10 Ravipati, C.B., Jackson, D.R., Xu, H.: 'Center-fed microstrip antennas with shorting vias for miniaturization'. Proc. IEEE Antennas and Propagation Society Int. Symp., 2005, vol. 3B, pp. 281–284
11 Weigand, S., Huff, G.H., Pan, K.H., Bernhard, J.T.: 'Analysis and design of broad-band single-layer rectangular U-slot microstrip patch antennas', *IEEE Trans. Antennas Propag.*, 2003, **51**, pp. 457–468
12 Sung, Y.J., Kim, Y.S.: 'An improved design of microstrip patch antennas using photonic bandgap structure', *IEEE Trans. Antennas Propag.*, 2005, **53**, pp. 1799–1804
13 Navarro, E.A., Craddock, I.J., Paul, D.L.: 'Synthetic dielectrics for planar antenna design', *Electron Lett.*, 2000, **36**, pp. 491–493
14 Navarro, E.A., Luximon, A., Craddock, I.J., Paul, D.L., Dean, M.: 'Multilayer and conformal antennas using synthetic dielectric substrates', *IEEE Trans. Antennas Propag.*, 2003, **51**, pp. 904–908
15 Wong, K.L., Wu, J.Y.: 'Single-feed small circularly polarized square microstrip antenna', *Electron. Lett.*, 1997, **33**, pp. 1833–1834
16 Huang, C.Y., Wu, J.Y., Wong, K.L.: 'High gain compact circularly polarized microstrip antenna', *Electron. Lett.*, 1998, **34**, pp. 712–713
17 Chen, W.S., Wu, C.K., Wong, K.L.: 'Novel Compact circularly polarized square microstrip antenna', *IEEE Trans. Antennas Propag.*, 2001, **49**, pp. 340–342
18 Yang, K.P., Wong, K.L.: 'Dual-band circularly polarized square microstrip antenna', *IEEE Trans. Antennas Propag.*, 2001, **49**, pp. 377–382
19 Sze, J.Y., Wong, K.L.: 'Slotted rectangular microstrip antenna for bandwidth enhancement', *IEEE Trans. Antennas Propag.*, 2000, **48**, pp. 1149–1151
20 Silvester, P.P., Ferrari, R.L.: 'Finite elements for electric engineers' (Cambridge University Press, New York, 1996, 2000, 3rd edn.), pp. 405–406
21 Ji, Y., Wang, H., Hubing, T.H.: 'A novel preconditioning technique and comparison of three formulations for the hybrid FEM/MoM method', *Appl. Comput. Electromagn. Soc. (ACES) J.*, 2000, **15**, pp. 103–114
22 Chew, W.C., Tong, M.S., Hu, B.: 'Integral equation methods for electromagnetic and elastic waves' (Morgan Claypool, USA, 2009), pp. 46–52
23 Lo, Y.T., Richards, W.F.: 'Perturbaton approach to design of circularly polarized microstrip antennas', *Electron. Lett.*, 1981, **17**, pp. 383–385
24 Haupt, R.L., Werner, D.H.: 'Genetic algorithms in engineering electromagnetics' (John Wiley Sons, Hoboken, NJ, 2007)
25 Weile, D.S., Michielssen, E.: 'Genetic algorithm optimization applied to electromagnetics: a review', *IEEE Trans. Antennas Propag.*, 1997, **45**, pp. 346–353
26 Haupt, R.L.: 'An introduction to genetic algorithms for electromagnetics', *Proc. IEEE Antennas Propag. Mag.*, 1995, **37**, (2), pp. 7–15
27 Goldberg, D.E., Deb, K.: 'Comparative analysis of selection schemes used in genetic algorithm', The Clearinghouse for Genetic Algorithms Tech Report No. 90007, The Univ. Alabama, Dept. Eng. Mech., Tuscaloosa, AL, 1991
28 Herscovici, N., Osorio, M.F., Peixeiro, C.: 'Miniaturization of rectangular microstrip patches using genetic algorithms', *IEEE Antenna Wirel. Propag. Lett.*, 2002, **1**, pp. 94–97
29 Ozgun, O., Mutlu, S., Aksun, M.I., Alatan, L.: 'Design of dual-frequency probe-fed microstip antennas with genetic optimization algorithm', *IEEE Trans. Antennas Propag.*, 2003, **51**, pp. 1947–1954
30 Altman, Z., Mittra, R., Boag, A.: 'New designs of ultra wide-band communication antennas using a genetic algorithm', *IEEE Trans. Antennas Propag.*, 1997, **45**, pp. 1494–1501
31 Altshuler, E.E.: 'Design of a vehicular antenna for GPS/IRIDIUM using a genetic algorithm', *IEEE Trans. Antennas Propag.*, 2000, **48**, pp. 968–972
32 See, C.H., Abd-Alhameed, R.A., Zhou, D., Excell, P.S., Hu, Y.F.: 'A new design of circularly-polarised conical-beam microstrip patch antennas using a genetic algorithm'. Proc. European Conf. Antennas and Propagations, EuCAP, France, 2006
33 Polivka, M., Drahovzal, M., Rohan, J., Hazdra, P.: 'Multiband patch antenna with perturbation elements generated by genetic algorithm'. Proc. European Conf. Antennas and Propagations, EuCAP, France, 2006

doi: 10.1049/iet-map.2010.0050